P4.7

ROTATIONAL EFFECTS ON FLOW AROUND IDEALIZED MOUNTAIN RIDGES

Helen Wells *, Stuart Webster and Andrew Brown
Met Office, Exeter, Devon U.K.

12th May 2004

1. INTRODUCTION

The parametrization of the effects of sub-gridscale orography (SSO) used in the Met Office Unified Model (Webster *et al.*, 2003) is very simple, using linear theory and ignoring rotation to predict the SSO drag. The use of such a simple prediction for the SSO drag was encouraged by the idealized experiments of Olafsson and Bougeault (1997, hereafter OB97) who found that when rotation was included the drag on an elongated mesoscale ridge (normalized by the prediction from linear theory ignoring rotation) depended only weakly on the low-level Froude number ($F_r = U/Nh_m$, where U is the low level wind speed, N is the buoyancy frequency and h_m is the height of the mountain), i.e. depended only weakly on the non-linearity of the flow. As illustrated in Webster *et al.*, even though the parametrization ignores rotation, it performs well in the UM with most of the drag being attributed to flow blocking, i.e. usually $F_r < 1$.

However, Shutts (1998, hereafter S98) suggested that the drag on a mesoscale mountain ridge should include a dependence on rotation, i.e. on f, the Coriolis parameter. This suggestion was based on a simple idealized model of the cold-air damming mechanism, which is the flow-blocking process captured by OB97 at low F_r, and is arguably also the dominant drag process over real mesoscale orography. Ultimately, S98 deduced an expression for the drag (F_{m*}, again normalized by the prediction from linear theory ignoring rotation) as follows:-

$$F_{m*} = \frac{\pi\gamma h_{m*}}{2(h_{m*}^2 + \gamma)}, \qquad (1)$$

where $\gamma = fL_e/u_0$ and $h_{m*} = Nh_m/u_0$. Here, L_e is the length of the mountain ridge and u_0 is the geostrophic wind speed perpendicular to the ridge. This model assumes that $L_e >> L_R$, where $L_R = Nh_m/f$ is the Rossby radius of deformation and hence also assumes that the Rossby number, $R_0 = u_0/(fL_x)$, based on the mountain half-width, L_x, is greater than unity, whilst the Lagrangian Rossby number $R_{0L} = V_b/fL_e$, where V_b is the barrier jet wind speed, is less than unity.

For typical values of L_e, u_0 and h_{m*}, Eq. (1) indicates that the normalized drag, F_{m^*}, may reach a maximum value of 3. Therefore S98 implies that the drag predicted by the current UM SSO parametrization may be up to a factor of 3 too small in certain situations.

The aim of this study is to extend the work of OB97 to clarify whether f should in fact be accounted for when parameterizing the drag due to SSO. The parameter space explored by OB97 is extended, principally through varying the ridge length. Using these simulations we test the predictions of the S98 model, in particular examining the drag predictions.

The numerical model and simulations performed are described in section 2. Section 3 describes the barrier jet which develops upstream of the ridge in our simulations. The pressure forces acting on the flow are discussed in section 4 before our findings are summarized in section 5.

2. THE NUMERICAL MODEL AND SIMULATIONS

The simulations in this study were performed using the three-dimensional, non-hydrostatic BLASIUS model described in Wood and Mason (1993). The model solves the time-dependent Boussinesq equations in a coordinate system whose model levels follow the terrain close to the ground but become horizontal near the top of the domain. The height of the surface was

$$h(x,y) = \begin{cases} h_m \left(1 + \left(\frac{x}{L_x}\right)^2 + \left(\frac{|y|-\eta}{L_y}\right)^2\right)^{-1.5} & |y| \geq \eta \\ h_m \left(1 + \left(\frac{x}{L_x}\right)^2\right)^{-1.5} & |y| < \eta \end{cases}, \qquad (2)$$

* Corresponding author address: Helen Wells, Met Office, Exeter, Devon, EX1 3PB, U.K.; email:helen.wells@metoffice.com

where η is the half-length of the flat section of the ridge and L_y is the half-length of the tapered ends of the ridge. L_x and L_y were fixed at 40km. This mountain shape corresponded to a flat ridge in the across-wind (y) direction, tapered at both ends by a witch of Agnesi shape. In the along-wind (x) direction the mountain had a witch of Agnesi shape. This mountain shape was chosen because it retains its height for most of it's length and is therefore similar to the ridge which S98 envisaged. In order to compare our results with those of other studies (e.g. OB97) we calculated the ridge length of a standard Agnesi mountain (i.e. $\eta = 0$) which would give the same linear drag as our mountain. Thus we consider our ridges to have an effective ridge length, L_e of $L_e = 2\eta + L_y$.

As our simulations were designed to test S98's drag predictions (our Eq: 1), γ was the main parameter varied. In the simulations γ was principally varied by increasing the ridge length, L_e, from 40 -1080 km. Additionally γ was varied by changing f and u_o from the basic setup of $f = 1 \times 10^{-4}$s^{-1} and $u_0 = 10$ms^{-1}. Most of the simulations had a free-slip lower boundary condition and $h_{m*} = 2.7$. In order to further explore the parameter space, simulations were also run with $h_{m*} = 5.4$. The sensitivity to friction was investigated by repeating a small subset of our simulations with a no-slip lower boundary condition. The simulations were run to 10^5s, by which time the drag force was varying by less than 10%.

3. THE BARRIER JET

A barrier jet is a mountain parallel wind which occurs on the upwind slope of a mountain. Barrier jets develop when the oncoming flow is decelerated by a high pressure region upstream of the mountain causing a net force to the left (in the northern hemisphere) as a result of geostrophic imbalance (Smith 1982). This imbalance forces a greater volume of air to flow round the northern end of the ridge (for westerly flow) creating a barrier jet. Figure 1 shows the velocity component, v, in the positive y (northward) direction for a free-slip run with $\gamma = 10.4$, $L_e = 520$km and $f = 2 \times 10^{-4}$s^{-1}. The barrier jet is clearly visible in Fig. 1 as a region of strong, positive v winds near the northern end of the ridge. In fact, the peak wind speed in the barrier jet was greater than u_0 in all of our simulations.

The characteristics of the barrier jet vary significantly between simulations. For example the maximum speed of the barrier jet increases from $1.5u_0$ to $4.1u_0$ when the ridge length is increased from

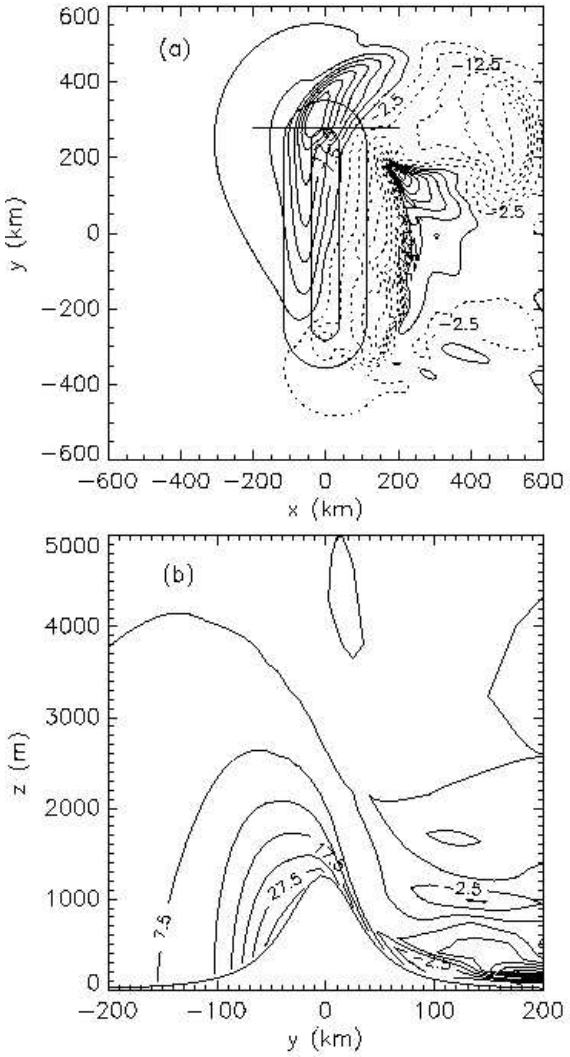

Figure 1: (a) is a plan view of the northward component of the wind, v. The thick solid lines are the mountain contours at 100m and 1000m respectively. (b) shows a cross-section of v at the northern end of the ridge (the position is indicated by the horizontal thick solid line on plot (a)) The contour interval is 5.0ms^{-1} with positive values denoted by solid lines and negative values denoted by dashed lines.

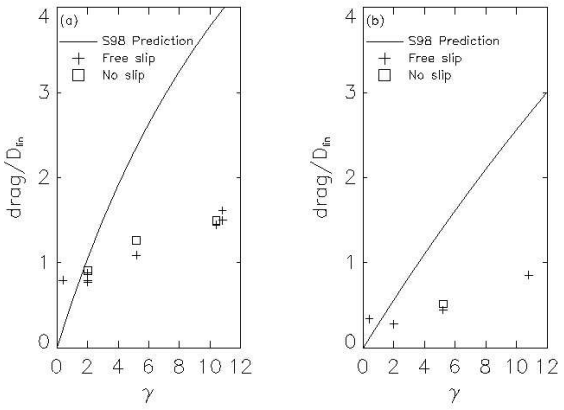

Figure 2: Normalized drag force in the model simulations and as predicted by S98 (our equation 1) plotted against γ for (a) $h_{m*} = 2.7$ (b) $h_{m*} = 5.4$.

40km to 1080km. The introduction of frictional effects substantially decelerates the barrier jet as well as raising the jet core off the surface.

4. PRESSURE FORCES ACTING ON THE FLOW

The pressure forces acting on the mountain can be separated into a drag force F_x which acts parallel to the incident flow and a lift force F_y which acts perpendicular to the incident flow. These forces are defined as

$$F_x = \int_{-\infty}^{\infty}\int_{-\infty}^{\infty} p' \frac{\partial h(x,y)}{\partial x} dxdy, \qquad (3)$$

$$F_y = \int_{-\infty}^{\infty}\int_{-\infty}^{\infty} p' \frac{\partial h(x,y)}{\partial y} dxdy, \qquad (4)$$

where p' is the pressure perturbation.

4.1 DRAG FORCE

One of the main aims of this study is to assess the impact of rotational effects on drag and to assess whether this impact is as large as the heuristic model of S98 suggests. Thus Fig. 2 shows the normalized modeled drag force plotted against γ for all the simulations performed. Note that the drag force is normalized by the drag prediction from linear theory.

It is clear from Figs. 2 (a) and (b) that the modeled drag force increases approximately linearly with γ. Thus a key result of this work is that it confirms S98's prediction that γ is a controlling parameter of the drag force in the blocked flow regime.

Comparison of Fig. 2(a) with Fig. 2(b) shows that the modeled drag force is also sensitive to h_{m*}, with smaller drag forces occurring for larger h_{m*}. This is consistent with OB97 who observed that the normalized drag decreased slightly for large h_{m*}. However, we find a much stronger dependence. For example our simulations show that when $\gamma = 2$ increasing the hill height from $h_{m*} = 2.7$ to 5.4 results in a 60% decrease in drag.

A comparison of the no-slip simulations with their free-slip equivalents indicates that frictional effects generally increase the drag force by about 15%.

Also shown in Fig. 2 is the drag force predicted by S98 (our Eq. 1) for each of the simulations. It is clear that the modeled dependence on γ is much weaker than that predicted by S98 and so as γ gets larger, the modeled drag force diverges more from Eq. 1. This discrepancy arises because, in order to get an estimate of total drag from his upstream cold air damming model, S98 assumed that the drag force downstream of the mountain was equal to the drag force upstream of the mountain (as the S98 model gives no information about the downstream flow conditions). Analysis of our results (not shown) reveals that the majority of the drag occurs upstream of the ridge axis and hence we find that S98 overestimates the dependence of the total drag force on γ. However, comparison of S98's prediction of the upstream component of the drag (i.e. 0.5*F_{m*}) with our simulations reveals that the S98 model was better at predicting the upstream component of the drag than predicting the total drag, although the dependence of the upstream drag force on γ was still overestimated by the S98 model.

4.2 LIFT FORCE

The lift force (Eq. 4) acts perpendicular to the incident flow and accounts for a significant proportion of the total pressure force in some of the simulations. The lift force arises due to asymmetry in the attached counter-rotating wake vortices as rotational effects cause the recirculation associated with the vortex attached to the northern end of the ridge to be strongest, leading to a southward directed force on the mountain. Note that the lift force in these simulations is not a drag force due to the turning of the incident wind, as it acts in the sense to accelerate the barrier jet rather than decelerate it.

An analysis of the variation in the lift force between different simulations (not shown) revealed that it does not scale on any of the relevant non-dimensional numbers. The lift force is most significant in the case of relatively short, high ridges with it reaching

60% of the amplitude of the drag force in a run with $h_{m*} = 5.4$ and $\gamma = 2.0$. In this case the total pressure force is rotated by 30^o from the direction of the incident wind.

5. SUMMARY

The primary aim of this work was to assess the impact of rotation on the drag forces experienced by flow impinging on long, high mountain ridges.

The pressure forces acting on the flow were investigated and the validity of S98's heuristic blocked flow model was assessed. This work verified that γ is a key non-dimensional parameter controlling the drag. Increasing γ caused the normalized drag to increase, but this increase was much less than that predicted by the S98 model.

A comparison of our results with those of OB97 revealed that the variation in normalized drag between low h_{m*} and high h_{m*} was much larger than their results suggested.

The implications of our results for the Webster *et al.* (2003) parametrization of subgrid-scale orographic drag are as follows. Most importantly the large variation in drag between simulations with low h_{m*} and high h_{m*} suggest that the parametrization should not ignore this variation (as it does currently). Additionally, our results suggest that representing the lift force in the parametrization may be necessary in order to get the direction of the total drag correct. This is most important in the case of short, high h_{m*} ridges where our simulations showed that the total force was rotated significantly from the direction of the incident wind.

Further details of this work are in Wells, Webster and Brown (submitted Q.J.R. Met. Soc.2004).

Ólafsson, H. & Bougeault, P. 1997: The effect of rotation and surface friction on orgraphic drag. *J. Atmos. Sci.* **54**, 193–210

Shutts, G. 1998: Idealized models of the pressure drag force on mesoscale mountain ridges. *Contr. Atmos. Phys.* **71**, 303–313

Smith, R. B. 1982: Synoptic observations and theory of orographically distributed wind and pressure. *J. Atmos. Sci.* **1982**, 60–70

Webster, S., Brown, A. R., Cameron, D. R. & Jones, C. P. 2003: Improvements to the representation of orography in the Met Office Unified Model. *Q. J. R. Meteorol. Soc.* **129**, 1989–2010

Wells, H., Webster, S. & Brown, A. R. submitted 2004: The effect of rotation on the pressure drag force produced by flow around long mountain ridges. *Q. J. R. Meteorol. Soc.*

Wood, N. & Mason, P. J. 1993: The pressure drag force induced by neutral, turbulent flow over hills. *Q. J. R. Meteorol. Soc.* **119**, 1233–1267